Bioaffinity Screening with a Rapid and Sample-Efficient Autosampler for Native Electrospray Ionization Mass Spectrometry

Author(s):
Kaeslin, Jérôme; Brunner, Cyrill; Ghiasikhou, Sahar; Schneider, Gisbert; Zenobi, Renato

Publication date:
2021-10-05

Permanent link:
https://doi.org/10.3929/ethz-b-000507526

Originally published in:
Analytical Chemistry 93(39), https://doi.org/10.1021/acs.analchem.1c03130

Funding acknowledgement:
178765 - Soft ionization mass spectrometry for studying noncovalent interactions (SNF)

Bioaffinity Screening with a Rapid and Sample-Efficient Autosampler for Native Electrospray Ionization Mass Spectrometry

Jérôme Kaeslin[†], Cyrill Brunner[†], Sahar Ghiasikhou[†], Gisbert Schneider[†], and Renato Zenobi[*,†]

[†] Department of Chemistry and Applied Biosciences, ETH Zürich, Vladimir-Prelog-Weg 3, CH-8093, Switzerland

ABSTRACT: Fast and efficient handling of ligands and biological targets are required in bioaffinity screening based on native electrospray ionization mass spectrometry (ESI-MS). We use a prototype microfluidic autosampler, called the "gap sampler", to sequentially mix and electrospray individual small molecule ligands together with a target protein and compare the screening results with data from thermal shift assay (TSA) and surface plasmon resonance (SPR). In a first round, all three techniques were used for a screening of 110 ligands against bovine carbonic anhydrase II (CAII), which resulted in five mutual hits and some false positives with ESI-MS, presumably due to the high ligand concentration or interferences from dimethyl sulfoxide (DMSO). In a second round, 33 compounds were screened in lower concentration and in a less complex matrix, resulting in only true positives with ESI-MS. Within a cycle time of 30 s, dissociation constants were determined within an order of magnitude accuracy consuming only 5 pmol of ligand and less than 15 pmol of protein per screened compound. In a third round, dissociation constants of five compounds were accurately determined in a titration experiment. Thus, the gap sampler can rapidly and efficiently be used for high-throughput screening.

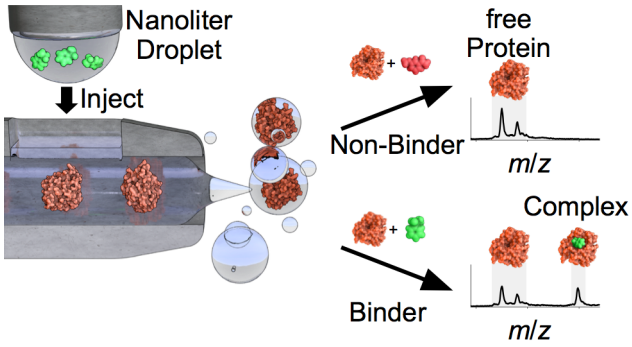

In small molecule drug discovery, scientists are searching for pharmaceutically suitable compounds that modulate the activity of a biological target.[1] Typically, this quest involves testing the target for binding against chemical libraries consisting of hundreds to millions of compounds in a process called high-throughput screening (HTS).[2] This challenge has to be addressed with analytical techniques which are fast, reliable and efficient in terms of costs and reagents. Biophysical methods based on a variety of principles are employed. The most commonly used include X-ray crystallography, nuclear magnetic resonance spectroscopy (NMR), surface plasmon resonance (SPR), thermal shift assay (TSA), isothermal titration calorimetry (ITC) and mass spectrometry (MS), each one with its individual advantages and disadvatages.[3] One particular MS approach detects a binding event by direct observation of target-ligand complexes. This so-called native/non-covalent MS is performed by electrospray ionization (ESI) MS, which is so soft that non-covalent interactions survive the ionization and the transfer from solution to the gas phase.[4,5] Reviews generally summarize the advantages of native MS as follows[3,6,7]: no labeling/immobilization required, low sample consumption and easily interpretable mass spectra that directly afford the binding stoichiometry. In contrast, disadvantages include false negative hits due to non-specific binding and the requirement of an ESI-friendly buffer, i.e., only volatile reagents and buffers can be electrosprayed.

Importantly, MS is generally so rapid and sensitive such that feeding the instrument quickly with low amounts of sample becomes the bottleneck for high speed analysis.[8] Various ESI[9-12] or ESI-derived[13-16] microfluidic autosamplers were developed to tackle this issue. However, most of these autosamplers were only used to analyze small molecules. Only the NanoMate[17,18] from Advion is commonly used to perform native MS with large molecules in a HTS setting. The NanoMate can sample 1–20 µl from a well plate with a disposable pipette tip. Next, the sample is delivered to a multi-nozzle nano-ESI chip and pushed into an inlet. Finally, the sample is electrosprayed with a 50–300 nl min^{-1} flow rate at a high voltage.

Zhang *et al.* were the first to use the NanoMate for bioaffinity screening based on native MS.[19] Since then, the NanoMate has been used numerous times for native MS bioaffinity HTS. However, there are only a handful of studies which directly compare automated native MS screening with alternative methods in terms of hit rate, quantification accuracy, cycle time and sample consumption. Benkestock *et al.* screened 23 ligands against the two human fatty acid bindings proteins H-FABP and A-FABP by NMR and native MS using the NanoMate.[20] MS was significantly faster, and hits were highly correlated between the two methods. Jecklin *et al.* quantified dissociation constant values K_D for 8 known inhibitors of human carbonic anhydrase comparing SPR, ITC and titration by native MS with the NanoMate.[21] MS was very time and sample efficient, but the K_D values diverged significantly between the three methods for some ligands. Maple *et al.* screened 157 compounds against the anti-apoptotic protein Bcl-x_L with the NanoMate and the results for 20 ligands were further validated with NMR and ITC.[22] Again, MS outperformed other methods significantly in terms of required time and sample, while having similar hit rates as NMR

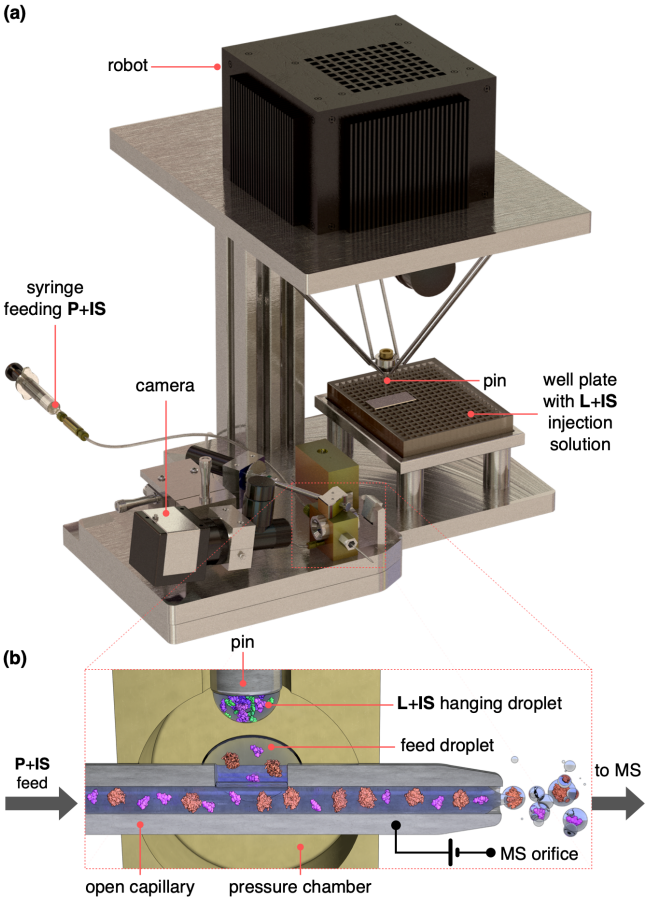

Figure 1. Overview of the gap sampler for native ESI-MS screening. (a) shows an overview of the gap sampler. (b) depicts schematically the moment of injection. The pin injects a **L**+**IS** containing hanging droplet into the **P**+**IS** containing droplet on top of the open capillary.

and K_D values comparable with ITC. Woods *et al.* screened 720 compounds against human carbonic anhydrase II with SPR and validated seven of these hits with X-ray crystallography and native MS using the NanoMate.[23] All seven SPR hits were also found with MS and six of them with X-ray crystallography. In a second round, 70 compounds were screened with SPR and MS: 24 were hits with both methods and 37 with at least one of the two indicating some false positives with SPR or MS. Using TSA and native MS with the NanoMate, Göth *et al.* screened four different proteins against 33, 16, 21 or 21 compounds, respectively.[24] Depending on the protein, the agreement between the methods was high (16 mutual hits) to very poor (0 mutual hits). 361 ligands were screened against endothiapepsin by Schiebel *et al.* with a biochemical assay, a reporter ligand displacement assay, NMR, TSA, MST, X-ray crystallography and native MS with the NanoMate.[25,26] The reported hit overlap between the techniques was remarkably low.

Beside the well-established NanoMate, Hoffmann-La Roche patented their own microfluidic ESI autosampler (figure 1).[27] This so called gap sampler was originally designed to pick up a few nanoliters of sample with a pin from a well plate and to inject it into the space between two capillaries positioned face-to-face to form a gap. A carrier liquid fed at a few µl min^{-1} through the first capillary bridged the gap to the second capillary, from which the liquid was constantly electrosprayed by application of a high voltage. An overpressure, which enclosed the two capillaries, prevented flooding. Thus, the sample injected into the liquid bridge is conveyed towards the end of the second ESI capillary. Meanwhile, the sampling pin is automatically washed and dried. This original setup was used for characterization studies involving small molecule flow injections[28], for automated non-specific extraction with a C_{18} solid phase[29] and for specific extraction using a protein modified extraction phase[30]. However, the gap sampler's operation was limited to carrier liquids with a high percentage of organic solvents to sustain the liquid bridge. Consequently, these denaturing conditions do not allow to analyze proteins in their native state. Additionally, the mixing of the nanoliter droplet with the microliters per minute flow rate lead to significant mixing and broadening of the sample plug.[31] However, it was shown to be advantageous to replace the two capillaries by a single capillary with an upwards oriented opening to allow access by the pin (figure 1(b)).[32]

In this article, we demonstrate that we can use the gap sampler with this kind of capillary for bioaffinity HTS based on native ESI-MS. The operating principle is as follows: a protein **P** is delivered through the open capillary. The pin picks up a ligand **L** from the well plate and injects it into the **P** feed (figure 1(b)). To quantify the amount of injected **L**, a nonbinding internal standard **IS** is spiked both into the **L** and **P** solution. **L**, **IS** and **P** are mixed inside the open capillary. The **L, IS** and **P** pass through the capillary within some residence time during which the **P** and **L** are incubated. Then, the **IS** concentration pulse is electrosprayed. At the same moment, a potential ligand protein complex [**P**+**L**] can be observed in the extracted ion chromatogram (XIC) (figure 2(a)). From the acquired mass spectra (figure 2(b) and (c)), where both bound and unbound **P** are observed, the K_D can be determined. With this method, the **P** and **L** mixing is performed automatically inside the open capillary. This has the advantage that unused **P** and **L** remain pure and can be used for another project or screening technique. Additionally, our autosampler does not require any disposable parts beside washing solvents which translates to low operating cost.

We test this method with a model system consisting of bovine carbonic anhydrase II (CAII) and a library of small molecules. In a first round, we qualitatively screen 110 ligands and compare the results with SPR and TSA. In a second round, we semi-quantitatively screen a smaller 33 compound library and compare K_D values of 10 binders with results from SPR. In a third round, we titrate five compounds to accurately determine the K_D values.

EXPERIMENTAL SECTION

Chemicals used. Water (H_2O, LC-MS grade, Merck), methanol (MeOH, OPTIMA LC/MS, Fisher Scientific), isopropanol (*i*PrOH, >99.5%, Fisher Scientific) and dimethyl sulfoxide (DMSO, 99.7%, Acros organics for MS, VWR chemicals for SPR) were used as solvents. Mass calibration was performed with Caesium iodide (CsI, Fluka). A 10 mM ammonium acetate (NH_4Ac, VWR) solution adjusted to pH 7.9 with ammonium hydroxide (Sigma Aldrich) was used as buffer for MS, a 10 mM phosphate buffered saline (PBS) solution supplemented with 5% DMSO for TSA and a 10 mM PBS with 0.05% *V/V* Polyoxyethylen(20)-sorbitan-monolaurat (Tween20) solution (PBS-T) for SPR. Bovine carbonic anhydrase II (CAII, Sigma Aldrich) was investigated as model protein **P**. As in previous work, tributylmethylammonium bromide (Bu_3MeNBr, abcr) served as nonbinding internal standard (**IS**) for MS.[28] For TSA, SYPRO Orange from Sigma Aldrich was used. For SPR, 1-

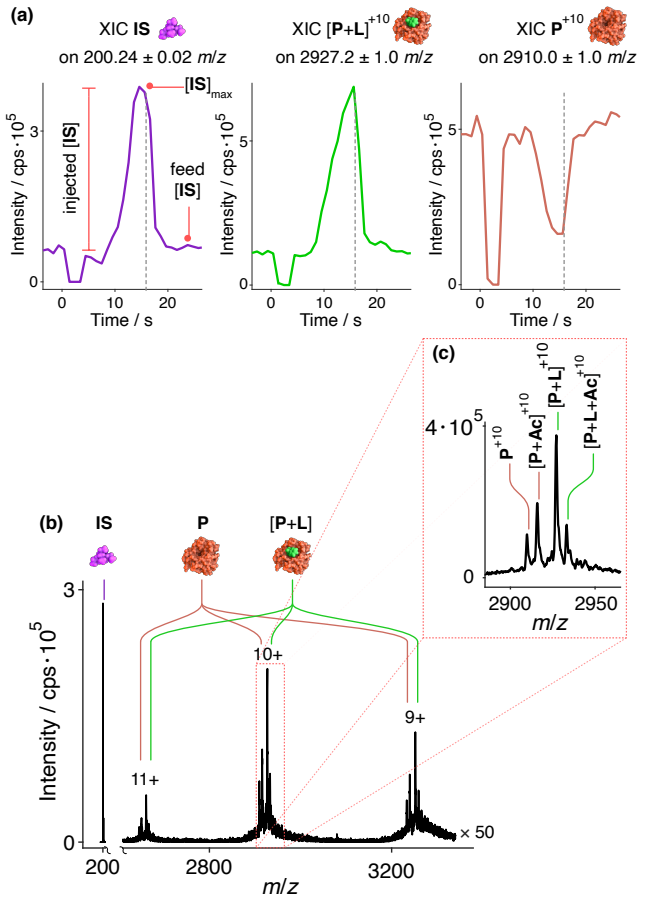

Figure 2. One exemplary injection cycle for binding ligand **A27** (a) shows the XIC during one injection cycle of a high affinity ligand for the nonbinding **IS**, the complex signal $[\mathbf{P}+\mathbf{L}]^{+10}$ and the free protein $\mathbf{P}^{+10}$. All XICs drop to zero during the injection because the spray becomes momentarily unstable. After a few seconds of residence time, the **IS** and $[\mathbf{P}+\mathbf{L}]^{+10}$ signals raise while the $\mathbf{P}^{+10}$ signal from the unbound protein is decreasing. The dashed line marks the point when the mass spectrum is read out for K_D calculation, i.e., where the bound to unbound ratio $\overline{R}$ is maximal. (b) shows exactly this mass spectrum. At low *m/z* the **IS** is observed and at high *m/z* different charge states of both bound and unbound **P** are visible. (c) shows a zoom into the region of the +10 charge state. **L** and acetate (**Ac**) complexes are observed.

ethyl-3-(3-dimethyl-aminopropyl)carbodiimide (EDC), *N*-hydroxysuccinimide (NHS), 1 M Ethanolamine solution, 10 mM acetate buffers pH 5.0 and High Capacity Amine Sensors (HCA) were bought from Bruker Daltonics (Hamburg, Germany). The names, structures and supplier informations of the ligands **L** are listed in the supporting information S1 (**A1** to **A111**) and S2 (**B1** to **B28**). Visually insoluble ligands in the stock solution were excluded in this study.

Sample Preparation for MS. A **P** stock solution was prepared by dissolving CAII in buffer. To minimize alkali metal ion adducts, the stock solution was buffer exchanged using spin columns (Micro Bio-Spin P-6 Gel Columns, SSC buffer, 6000 Da limit, Bio-Rad) preconditioned with NH_4Ac buffer. Subsequently, [**P**] was quantified by UV/Vis (NanoDrop 2000, Thermo Scientific) with an extinction coefficient ε_{280} = 50 400 M^{-1} cm^{-1}.[33] Thereafter, the stock solution was diluted to the target concentration $[\mathbf{P}]_0$ (typically 3 to 7 µM) with NH_4Ac buffer. During this dilution step, the **IS** in NH_4Ac buffer was spiked to get the desired [**IS**] (typically 0.5 to 2 µM).

For the ligands, 5 to 100 mM **L** stock solutions in DMSO were prepared and subsequently diluted to the desired concentration for injection (typically 100 µM to 3 mM) with either DMSO or buffer. During this dilution step, the **IS** in NH_4Ac buffer was spiked in a known ratio to the **L** (typically 1:1 to 3:1). Prior to analysis, 40 µl of this **L** solution was filled into a 384 microwell plate.

Gap Sampler Operation. A detailed description on the gap sampler's design[27,34] and hardware[28] can be found in previous work. Instead of the original setup with an inlet and an outlet capillary, a laser ablation machined open capillary (schematically shown in figure 1(b)) was used. The open capillary was recently presented and characterized.[32] Furthermore, the gap sampler's desolvation performance during ESI was improved by mounting a coaxial sheath gas (250 l h^{-1} N_2) around the open capillary's end (details in figure S3).

The **P** was constantly fed through the open capillary (typically with 2.5 to 4 µl min^{-1}). To prevent flooding out of the open capillary's middle opening, an overpressure was applied (typically 40 mbar to 120 mbar). For ESI, a capillary voltage of 2.8 to 4 kV was applied. To achieve a stable liquid flow and an efficient ionization, the flow rate, overpressure and capillary voltage were tuned every day prior to measurements.

For the **L** sampling, a 229 µm diameter pin picked up a hanging droplet of a **L** solution from the well plate. Subsequently, the pressure chamber was opened for injection. The overpressure loss to atmospheric pressure (from >40 to 0 mbar) caused flooding of the feed solution such that a small droplet formed on top of the open capillary (figure 1(b)). As a consequence, the electrospray faded out because no more feed solution was delivered to the capillary's end. During this time, the detected MS signal dropped to zero. Meanwhile, the pin was inserted into the pressure chamber and injected the **L** hanging droplet into the **P** containing droplet on the capillary's top. After injection, the pin was pulled out of the pressure chamber and the pressure valve closed. As a result, the overpressure built up again and pushed the droplets back into the capillary. The liquid flow restabilized and the potential [**P**+**L**] complex was ionized after a few seconds of residence time in the open capillary. An example of such an injection cycle together with a schematic, the time resolved MS signal as well as the camera's view on the open

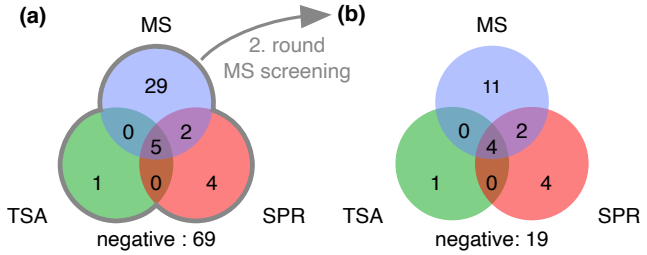

Figure 3. (a) First round screening: Venn diagram representing the hits from the first round screening of **A1**-**A111** with TSA, SPR and the gap sampler measured from a 3 mM **L** solution on the well plate. **A98** was removed from the set because it was insoluble for SPR and TSA compatible concentrations. (b) Second round screening: Venn diagram representing the hits after rescreening the first round hits at lower concentration and with no DMSO in the capillary feed. The precipitating **A29** was not rescreened but assumed to be an MS hit from the first round. Compound information is listed in table S1.

capillary can be found in figure S4. The XICs of an exemplary injection are also shown in figure 2(a). After the injection, the pin was automatically washed by 50:50 MeOH:H_2O and 50:50 *i*PrOH:H_2O (each typically 2 to 6 s) and dried by nitrogen (typically 2 to 6 s). The typical cycle time was 20 to 40 s depending on the flow rate and washing time.

Mass Spectrometry. ESI-MS was performed in positive mode on a Synapt G2 HDMS (Waters). Prior to installation of the gap sampler onto the MS, a CsI cluster (40 mg ml^{-1} in H_2O) mass calibration was performed using a commercial nano-ESI source with Au/Pd-coated glass capillary emitters (Thermo Scientific).

For native ESI-MS with the gap sampler, the instrument was run in Q-TOF (no ion mobility) and resolution (single-pass TOF) mode in the 100 to 5000 *m*/*z* mass range. The scan time was set to 1 s. The *auto* quadrupole profile was selected to have high transmission for the whole mass range. The MS parameters were tune for soft and sensitive ion transmission. The following parameters were selected: Sampling cone 0 V, source offset 0 V, source temperature 30 °C, trap collision energy voltage 2 V, trap gas flow 5.5 ml min^{-1} and transfer collision energy voltage 1 V.

MS Data Treatment. Spectra were recorded with MassLynx 4.0 (Waters). The .raw data was converted to .mzXML files using msconvert[35] and then processed by Matlab R2018a (MathWorks).

For quantification of the dissociation constant K_D, the following formula was used:[36]

$$K_D = \frac{[\mathbf{L}]_{max} - \frac{\bar{R}}{1+\bar{R}}[\mathbf{P}]_0}{\bar{R}}$$

$[\mathbf{L}]_{max}$ is the maximum ligand concentration in the concentration pulse after an injection. $[\mathbf{L}]_{max}$ was determined by the maximum **IS** concentration $[\mathbf{IS}]_{max}$ since they were injected in a known ratio (Figure S4(h)). $[\mathbf{IS}]_{max}$ was determined by a standard addition during the injection of the **L** and **IS** containing hanging droplet into the **P** and **IS** containing feed droplet. In the above formula, $[\mathbf{P}]_0$ is the free protein concentration which corresponds to the feed concentration. Dilution upon injection was neglected since only a nl droplet is injected into a µl min^{-1} flow. The parameter $\bar{R} = \overline{I([\mathbf{P}+\mathbf{Ac}_q+\mathbf{L}]^{+n})/I([\mathbf{P}+\mathbf{Ac}_q]^{+n})}$ is the charge state averaged intensity ratio of bound to unbound protein **P** considering q=0,1,2 acetate (**Ac**) adducts. $\bar{R}$ is determined from the mass spectrum with the highest proportion of bound protein in a time series of mass spectra, i.e., where $[\mathbf{L}]_{max}$ is reached. This means that the spectrum used to calculate the K_D therefore was acquired only for the set scan time (1 s). Such an exemplary spectrum is shown in figure 2(b) and (c). This spectrum was smoothed, baseline subtracted, and the corresponding peaks were integrated to calculate $\bar{R}$ and consequently K_D.

Alternatively, K_D was determined by titration in some experiments. In this case, different concentrations of **L** were injected into a constant [**P**] feed. $\bar{R}$ is then plotted against $[\mathbf{L}]_{max}$. K_D was determined by a least squares regression with the following formula:[21,37]

$$\bar{R} = \frac{\frac{[\mathbf{L}]_{max} - [\mathbf{P}]_0 - K_D}{K_D} + \sqrt{4\frac{[\mathbf{L}]_{max}}{K_D} + \left(\frac{[\mathbf{L}]_{max} - [\mathbf{P}]_0 - K_D}{K_D}\right)^2}}{2}$$

TSA and SPR experimental. The sample preparation and methodology for TSA and SPR followed the standard approach described in the supporting information.

RESULTS AND DISCUSSION

Qualitative Screening. In a first experiment, we investigated the gap sampler's performance for qualitative and rapid hit detection as often encountered in a first screening round during drug discovery. This implies that the library might contain weak binders only detectable at high **L** concentrations. In such a screening, DMSO is the preferred solvent due to its dissolving ability[38], which on the downside might introduce artifacts in ESI. Thus, our model library, consisting of compounds **A1** to **A111,** was filled into the well plate as a 3 mM **L** and 600 µM **IS** solution in 94:6 DMSO:buffer. Upon injection with the gap sampler, the **L** solution is expected to be significantly diluted to minimize the effect of DMSO. The open capillary was fed with 3 µM **P** and 0.5 µM **IS** in 2:98 DMSO:buffer at a flow rate of 3 µl min^{-1}. The 2% DMSO in the open capillary are used to wash out any **L** precipitate in case an insoluble compound were injected. However, the DMSO and the high **L** concentration led to charge state shifts and ion suppression during injection. Consequently, accurate quantification of the binding affinity was not possible. Despite the ESI artefacts, we assumed that both the bare and the bound protein suffer equally from ion suppression. Thus, we nonetheless determined a calculatory-K_D to define an affinity cut-off for binders at 100 µM. Since many ligands also showed multiple non-specific adducts, complex signals [**P**+**L**$_n$] with up to n=3 ligands together with the **Ac** adducts were taken into account. No calculatory-K_D was determined for ligand **A29** because it precipitated in the open capillary but was clearly binding (see depletion of $\mathbf{P}^{+10}$ XIC in figure S5). Fortunately, **A29** didn't clog the open capillary and thus waiting and flushing **A29** out was sufficient to resolve the problem. For the reference measurements with TSA, a melting temperature cut-off of ΔT_m > 1.5 °C was selected, which corresponds to the five-fold sum of the mean and standard deviation of the negative control **A24**.[39] Likewise, the SPR cut-off was set to the threefold of the highest observed mean normalized signal of **A24**. The experimental values for SPR, TSA and MS can be found in table S1, the XICs in figure S5, the mass spectra in figure S6 and the SPR sensorgrams in figure S7.

The Venn diagram in Figure 3(a) shows the TSA, SPR and MS hits. All three methods identify five hits, all of which contain a sulfonamide moiety that mediates the binding to CAII. However, all methods detected a few compounds uniquely, i.e., TSA found 1 uniquely, SPR 4 and the gap sampler 29. Particularly the gap sampler seems to detect a significant number of false positives. Presumably, this is due to some compounds forming significant amounts of non-specific adducts as can be observed by the Poisson-like distribution of multiple **L** adducts[40] (figure S6). The same problem with false positives was also reported in the NanoMate HTS studies mentioned above.[24,25] Non-specific binding might be enhanced at high **L** concentration or with the presence of DMSO, which was reported to alter binding strength in ESI.[41]

To reduce the effect of non-specific binding, the first round positive hits found by TSA, SPR and the gap sampler were re-screened in a second round (assuming the precipitating **A29** to be binding, ignoring insoluble **A98**). This time, the 41 compounds were injected three times from a 600 µM **L** and 600 µM **IS** in 12:88 DMSO:buffer solution into a stream of 5.5 µM **P**

and 0.5 µM **IS** in 100% buffer. While the charge state shift upon injection was still observed (figure S8), non-specific adducts were less problematic this time (figure S9) and thus the affinity cut-off was set to 400 µM. Figure (b) shows the adapted Venn diagram, where the supposedly false positives are reduced from 29 to 11. Four compounds are detected with all three methods.

Table 1. Ligand (**L**) amount, protein (**P**) amount and time requirements for the three methods used in this manuscript for one qualitative measurement only, i.e., ignoring repetitions. Values represent estimates for the methods and instruments used in this study and might deviate from values with other equipment.

	TSA	SPR	Gap sampler
L (pmol)	1250	6250	10
P (pmol)	40	in total 670	10
time (s)	50	620	35

TSA detects **A91** as a hit which is neither detected by SPR nor the gap sampler. **A91** presumably exhibits an aggregation phenomenon in TSA which can be concluded from the relatively large difference between the duplicated TSA measurements. The gap sampler seems to outperform TSA regarding false negatives because it detects **A78** and the sulfonamide bearing ligand **A121** together with SPR. In contrast, SPR is the only method that detects the compounds **A50**, **A92**, **A106** and **A110**. **A50** and **A92** might be false positives in SPR since the rectangular sensorgram indicates non-specific binding. Thus, the sulfonamide bearing and SPR hits **A106** and **A110** are presumably false negatives with the gap sampler. We hypothesize that these false negatives arise from kinetic limitations. Since the kinetic constants k_{on} and k_{off} are known from the SPR experiment (table S1), the binding kinetics can be modeled and a time-dependent apparent pre-equilibrium $K_D(t)$ constant can be computed (figure S10). Reading the $K_D(t)$ for the t=24 s residence time through the open capillary shows that successfully identified MS hits are near the equilibrium or at least have an apparent $K_D(t)$ in the range of a few tens of µM. In contrast, the false negatives **A106** and **A110** have a significantly higher apparent $K_D(t)$ and therefore did not form enough complex to be detected. Hence, under these conditions, the gap sampler is limited to systems which equilibrate sufficiently rapidly to reach a detectable apparent $K_D(t)$ within 24 s. Nonetheless, we conclude that the gap sampler performs well with regard to false negatives because all TSA or SPR hits not detected by MS can be explained by either being a TSA/SPR artefact or by kinetic constraints. Controlling false negatives is crucial in the early drug discovery phase because false positives are discarded later in the process while false negatives are permanently lost in a drug discovery campaign.

With a cycle time of 35 s per **L** for these experiments, the gap sampler outperforms the 50 s of TSA (96 well plate in 81 min) and the 620 s of SPR. These numbers correspond to the experimental time required in this study for one repetition only (see table 1). Larger TSA well plates or newer SPR instruments can lead to shorter cycle times for these reference methods. With the gap sampler, 5 pmol **P** per tested **L** were used in the first screening round and 10 pmol **P** in the second round. Meanwhile, the **L** consumption was 10 or 6 pmol, respectively. For comparison, SPR consumes 6250 pmol **L** per measurement and 670 pmol **P** in total since SPR is non-destructive regarding **P**. For

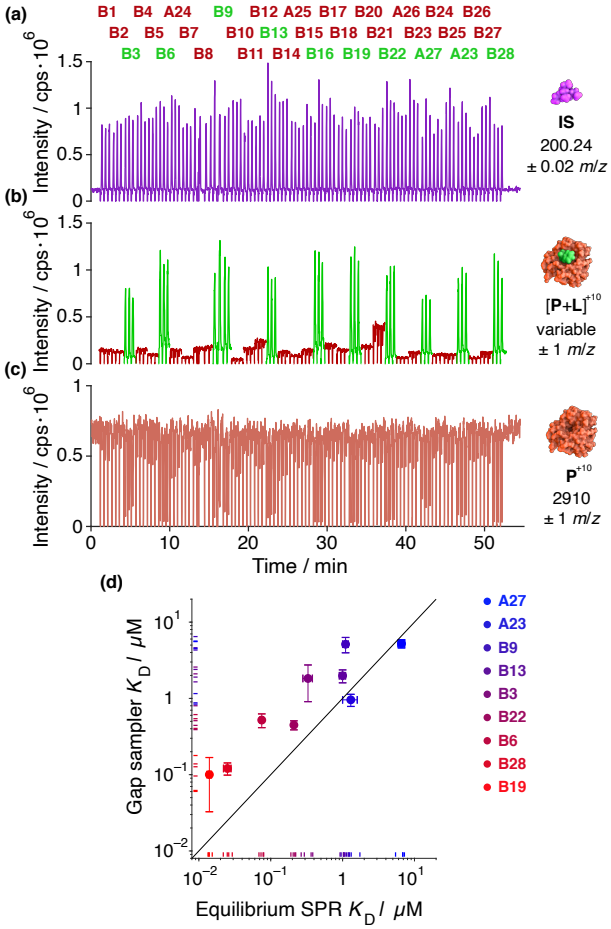

Figure 4. Screening of a 33 **L** set with three repetitions. (a) The XIC of the **IS**, which present both in-line in the **P** feed as well as in the injected **L** solution. The representation and color coding is identical to figure 2(a) but for multiple ligands with 3 repetitions, each. (b) The XIC at the mass, where the complex $[\mathbf{P}+\mathbf{L}]^{+10}$ would be observable if a binder was injected. Due to spray instability, **B9** was injected four instead of three times. (c) The XIC of the unbound $\mathbf{P}^{+10}$. (d) Comparison of K_D values determined by SPR and by the gap sampler. The dots represent average±standard deviation and the ticks on the axes are the individual values.

TSA, the consumption was 1250 pmol **L** and 40 pmol **P** per measurement. A major advantage of the gap sampler is the fact that **P** and **L** are mixed inside the open capillary. This means that the last step of the sample preparation is done on-line, which minimizes work and unrecoverable **P** and **L**. Undoubtedly, this is an advantage because unused **L** on the well plate could be used for another screening project by simply changing the target in the feed solution.

In summary, we conclude that the gap sampler performs well for rapid screening. Speed, sample efficiency and reliable true positive detection are the main advantages. Limitations are found for **L** and **P** combinations which do not bind sufficiently rapidly within the residence time of 24 s. Additionally, multiple false positives were found, presumably due to high **L** concentration or due to the high DMSO content.

Semi-quantitative screening. To assess the gap sampler's performance in more detail, a smaller 33 ligand library was screened, including the previously used **A23** to **A27** as well as **B1** to **B28** (table S2). The requirement for all of them is that

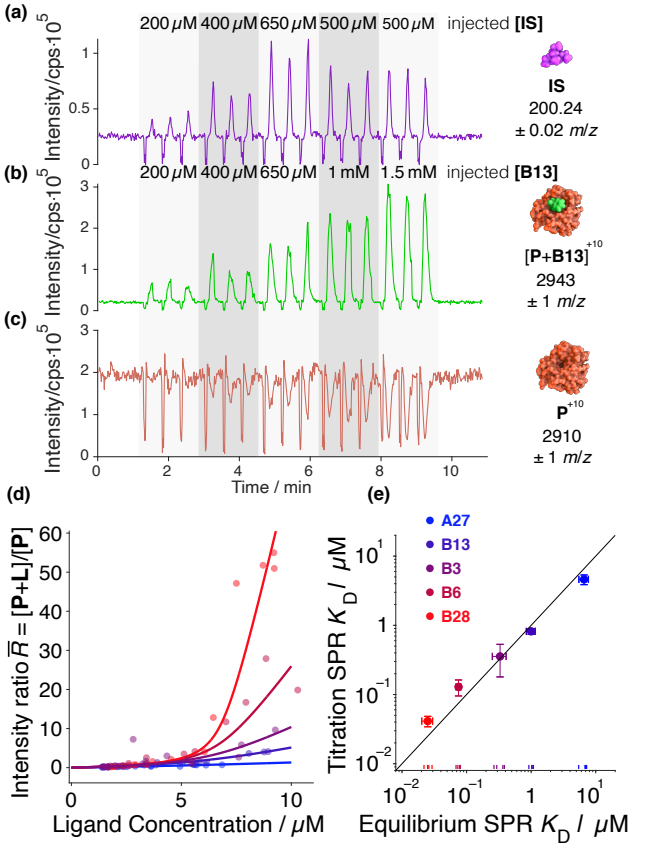

Figure 5. K_D Quantification by titration. (a) The XIC of the **IS** during **B13** injection. (b) XIC of $[\mathbf{P}+\mathbf{B13}]^{+10}$ with increasing concentration. (c) XIC of unbound $\mathbf{P}^{+10}$. (d) concentration dependence of the bound to unbound ratio $\bar{R}$ for the five compounds. (e) K_D values determined by regression compared with the values from SPR. *x*-error bars are the 95% confidence interval of repetitions, which are shown as ticks on the axis. *y*-errors bars mark 95% confidence interval of the estimate K_D calculated based on the residuals from (d).

they are soluble in NH_4Ac buffer. Ten compounds were expected to bind due to their sulfonamide group, which is known to interact with CAII.[42] The other 23 compounds were chosen arbitrarily as negative controls. A 6.24 µM **P** and 1.76 µM **IS** solution was fed with 4 µl min^{-1} through the open capillary. The 600 µM **L** and 600 µM **IS** solutions were injected three times from the well plate into the open capillary. Figure 4(a) shows the **IS** XIC, from which $[\mathbf{L}]_{max}$ is calculated. The determined $[\mathbf{L}]_{max}$ was 15 µM on average. Thus, we estimate that the mean total amount of **L** injected is 5 pmol or 8.3 nl of the 600 µM **L** solution. With the higher flow rates used here, the gap sampler's operating figures were: 30 s cycle time, 5 pmol **L** and 13 pmol **P** consumed per injection. Figure 4(b) shows the XIC at the *m/z*, where the complex $[\mathbf{P}+\mathbf{L}]^{+10}$ would be expected if a binding **L** was injected. Figure 4(c) depicts the XIC of the unbound $\mathbf{P}^{+10}$.

Qualitatively, all sulfonamide bearing ligands can be identified as binders by the peak in the $[\mathbf{P}+\mathbf{L}]^{+10}$ XIC and by the unbound $\mathbf{P}^{+10}$ depletion, observable in the corresponding XIC. At the same time, none of the other ligands shows a response in the $[\mathbf{P}+\mathbf{L}]^{+10}$ XIC, highlighting that they are non-binders. Thus, all 10 sulfonamide compounds were hits while all 23 negative controls were non-binding. Hence, when working at lower **L** and DMSO concentrations, an excellent true positive hit rate was observed while there was no more problem with false positives. Additionally, there was no charge state shift observed anymore caused by DMSO. Remarkably, the gap sampler outperformed SPR here regarding true positives: sulfonamide bearing **B16**, which was previously reported to be binding[43], was a hit with the gap sampler and TSA but not with SPR.

Taking the $[\mathbf{P}+\mathbf{L}]^{+10}$ XIC signal as a response for binding, a screening figure of merit called *Z'* can be calculated.[44] It describes the statistical significance of a screening assay by comparing the response of a positive and a negative ligand. If $0.5 \leq Z' \leq 1$, a screening qualifies as excellent. Here, the binders **B6** and **B13** were compared with the nonbinding **A25**, which yielded in $Z' = 0.82$ and $Z' = 0.73$, respectively (figure S11). In fact, the binders were very well separated from nonbinders and the $[\mathbf{P}+\mathbf{L}]^{+10}$ signal for one individual **L** showed a low standard deviation. Notably, the $[\mathbf{P}+\mathbf{L}]^{+10}$ XIC maximum has a lower standard deviation than the **IS** XIC. This indicates that accuracy of the K_D quantification's presumably will be limited by the **IS** quantification.

From the binder's mass spectra (figure S12), the K_D values were determined by using the K_D formula. The weakest binder was the SPR false negative **B16** with a K_D value of 6.6 µM and 2.0 µM standard deviation. The K_D values of the other 9 binders are compared with SPR in Figure 4(d) (values in table S1 and S2, sensorgrams in figure S13). On average, K_D values are a factor of 3.9 higher with the gap sampler compared to SPR. Thus, the gap sampler tends to underestimate the binding of the ligands. Again, we hypothesize that this is due to kinetic limitations. However, modelling of with the k_{off} and k_{on} kinetic constants from the SPR data indicates that only the K_D of **A23** and **B3** is overestimated by more than 10% because equilibrium is not reached within the 12 s residence time in the open capillary (figure S14). Consequently, kinetic limitations do not fully explain the K_D discrepancy. Other explanations for the discrepancy might be (1) distorted SPR K_D values due to **P** immobilization, (2) incomplete mixing in the open capillary, i.e., **P**, which is not in contact with sufficient **L**, seems to be non-binding, leading to an overestimated K_D or (3) insufficient time resolution with a 1 s scan time, i.e., the actual highest bound to unbound ratio $\bar{R}$ in a **L** concentration pulse is not captured correctly. In fact, we found that the K_D overestimation is significantly worse when 3 s of mass spectra were averaged instead of 1 s, i.e., the assumption that the maximum observed $\bar{R}$ is caused by the observed $[\mathbf{L}]_{max}$ becomes invalid. Consequently, quantification at high flow rates might be restricted by how accurately the bound to unbound ratio $\bar{R}$ can be time resolved. The relatively high fluctuations of the gap sampler presumably arise from a trade-off between accuracy and precision depending on the selected time resolution: On the one side, it is important to catch the peak apex of a **L** and **IS** concentration pulse for correct K_D determination. On the other side, using only a single scan (duration 1 s) to determine $\bar{R}$ introduces fluctuations from the electrospray to the K_D determination.

In conclusion, with MS-friendly solvents, the gap sampler shows great screening capabilities regarding the hit rate as well as *Z'*. Quantitatively, the binding strengths are underestimated with the gap sampler. However, the values match within one order of magnitude and fit well in their relative order with the exception of **A23** (figure S15). Thus, the gap sampler is suitable to estimate a dissociation constant within an order of magnitude rapidly and sample-efficiently.

Quantification via titration. For all experiments described so far, **L** and **P** were mixed at a fixed ratio. Alternatively, they can

be mixed at different ratios and by a least squares regression, the K_D value can be determined. This titration approach, which is known to give more accurate results[22,24], was performed for the compounds **A27**, **B13**, **B3**, **B6** and **B28** covering a broad affinity range. For this experiment, 6.91 µM CAII and 0.79 µM **IS** were fed at 3.5 µl min^{-1} through the open capillary. Solutions with an increasing **L** concentration and a known **L** to **IS** ratio were injected. Each compound was injected at five different concentrations with three repetitions. As an example, the 15 point titration of **B13** is shown in Figure 5(a) to (c) (other ligands in figure S16). With increasing **B13** being injected, more [**P**+**L**]$^{+10}$ is observed in the XIC and more unbound **P**$^{+10}$ is depleted. From the mass spectra in figure S17, the ratio of bound to unbound protein $\overline{R}$ can be determined as a function of $[\mathbf{L}]_{max}$. This dependence is shown for all the five compounds in Figure 5(d) together with the titration curve obtained from a least squares regression for the K_D value. These K_D values are compared with the SPR K_D values in Figure 5(e).

Using titration for quantifying K_D yields in more accurate results. The 15 measurements per ligand during one titration experiment compensate the large standard deviation for one individual measurement. On average, the K_D determined with the titration is overestimated by only 20%. The deviation is more pronounced for the strongly binding ligands **B6** and **B28**. Quantification for these ligands tends to be difficult because the unbound protein signal, used to calculate $\overline{R}$, is almost completely depleted. While the titration yields in accurate quantification, it consumes significantly more sample, i.e., roughly 190 pmol **P** and 20 pmol **L** for one titration experiment. Additionally, one titration experiment requires approximately 8 min.

Therefore, the gap sampler can quantify K_D values with an accuracy comparable to SPR. However, this requires higher amounts of **P** and **L** as well as more time. Consequently, this approach is more suitable for a second round profiling than for a first round rapid screening.

CONCLUSIONS

In conclusion, we demonstrated that the gap sampler is a promising autosampler for high throughput bioaffinity screening based on the noncovalent detection of protein ligand [**P**+**L**] complexes by electrospray ionization mass spectrometry. In under 40 s and with less than 15 pmol of protein and ligand consumed per tested compound, a library of 110 small molecules was screened against bovine carbonic anhydrase II. Sample handling is minimized because protein and ligand are mixed inside the electrospray capillary. This on-line incubation makes the unused ligand solutions on the well plate and protein solution in the syringe fully recoverable for the next screening steps. Screening involving ligands at high concentration and dissolved in DMSO is possible but might increase the number of false positives due to formation of non-specific adducts. Additionally, the autosampler's high throughput compromises the method's use for ligands with slow binding kinetics, which is an inherent problem for fast techniques. By using lower ligand concentrations and volatile buffer, the problem with non-specific adducts was circumvented and the gap sampler detected all true positives and true negatives from a 33 small molecule library. Dissociation constants lie within the same order of magnitude as those obtained by surface plasmon resonance and, more importantly, follow the same ranking. In titration experiments requiring more sample and time, accuracies with a mean difference of 20% were obtained.

Benchmarking the gap sampler with reference techniques like thermal shift assay or surface plasmon resonance showed that the gap sampler has a similar or even better performance in terms of speed, sample consumption and hit detection. Future developments of the prototype might help to improve these figures. First, an aspiration instead of an overpressure setup could allow faster injection rates. Second, the protein could be fed in concentration pulses, which would reduce the protein consumption. Third, feeding a protein incubated with a reporter ligand, which is replaced upon injection of the ligand under investigation, would help to distinguish nonspecific from specific binding which would reduce false positives.

ASSOCIATED CONTENT

Supporting Information

The Supporting Information is available free of charge on the ACS Publications website.
tab. S1: **A1**-**A111** information, tab. S2: **B1**-**B28** information, experimental section TSA/SPR, fig. S3: MS: gap sampler modifications, fig. S4: MS: injection cycle overview, fig. S5: MS: **A1**-**A111** first qualitative screening, fig. S6: MS: **A1**-**A111** spectra first qualitative screening, fig. S7: SPR: **A1**-**A111** sensorgrams, fig. S8: MS: second qualitative screening, fig. S9: MS: spectra second qualitative screening, fig. S10: MS: binding kinetics qualitative screeening, fig. S11: MS: Z' factor, fig. S12: MS: **A23**-**A27**/**B1**-**B28** spectra semi-quantitative screening, fig. S13: SPR: binder sensorgrams semi-quantitative screening, fig. S14: MS: binding kinetics semi-quantitative screeening, fig. S15: MS: ranking semi-quantitative screeening, fig. S16: MS: **A27**/**B3**/**B6**/**B28** titration, fig. S17: MS: **A27**/**B3**/**B6**/**B13**/**B28** titration spectra

AUTHOR INFORMATION

Corresponding Author

* E-mail: zenobi@org.chem.ethz.ch.

Notes

G. Schneider declares a potential financial conflict of interest as a co-founder of inSili.com LLC, Zürich, and a consultant to the pharmaceutical industry. The other authors declare no competing financial interest.
The original data used in this publication are made available in a curated data archive at ETH Zürich (https://www.reasearch-collection.ethz.ch) under the DOI 10.3929/ethz-b-000494717.

ACKNOWLEDGMENT

The authors thank Dr. Christof Fattinger, Dr. Adrien Marchand, Roger Steiner and Martin Köhler. J. Kaeslin acknowledges a fellowship from the Scholarship Fund of the Swiss Chemical Industry (SSCI). S. Ghiasikhou acknowledges the financial support by the Swiss National Science Foundation (grant no. 200020_178765).

REFERENCES

(1) Blass, B. *Basic principles of drug discovery and development*; Academic Press: Amsterdam, 2015.
(2) Hüser, J.; Mannhold, R.; Kubinyi, H.; Folkers, G. *High-throughput screening in drug discovery*; Wiley-VCH: Weinheim, 2006.
(3) Renaud, J.-P.; Chung, C.-W.; Danielson, U. H.; Egner, U.; Hennig, M.; Hubbard, R. E.; Nar, H. Biophysics in drug discovery: impact, challenges and opportunities, *Nat. Rev. Drug Discov.* **2016**, *15*, 679-698.
(4) Loo, J. A. Studying noncovalent protein complexes by electrospray ionization mass spectrometry, *Mass Spectrom. Rev.* **1997**, *16*, 1-23.

(5) Hofstadler, S. A.; Sannes-Lowery, K. A. Applications of ESI-MS in drug discovery: interrogation of noncovalent complexes, *Nat. Rev. Drug Discov.* **2006**, *5*, 585-595.
(6) Holenz, J. *Lead Generation: Methods, Strategies, and Case Studies*; Wiley-VCH: Weinheim, 2016.
(7) Renaud, J.-P.; Delsuc, M.-A. Biophysical techniques for ligand screening and drug design, *Curr. Opin. Pharmacol.* **2009**, *9*, 622-628.
(8) McLafferty, F. W. Tandem mass spectrometry, *Science* **1981**, *214*, 280-287.
(9) Felten, C.; Foret, F.; Minarik, M.; Goetzinger, W.; Karger, B. Automated high-throughput infusion ESI-MS with direct coupling to a microtiter plate, *Anal. Chem.* **2001**, *73*, 1449-1454.
(10) Pei, J.; Li, Q.; Kennedy, R. T. Rapid and label-free screening of enzyme inhibitors using segmented flow electrospray ionization mass spectrometry, *J. Am. Soc. Mass Spectrom.* **2010**, *21*, 1107-1113.
(11) Jin, D. Q.; Zhu, Y.; Fang, Q. Swan probe: A nanoliter-scale and high-throughput sampling interface for coupling electrospray ionization mass spectrometry with microfluidic droplet array and multiwell plate, *Anal. Chem.* **2014**, *86*, 10796-10803.
(12) Özbal, C. C.; LaMarr, W. A.; Linton, J. R.; Green, D. F.; Katz, A.; Morrison, T. B.; Brenan, C. J. High throughput screening via mass spectrometry: a case study using acetylcholinesterase, *Assay Drug Dev. Technol.* **2004**, *2*, 373-382.
(13) Murata, T.; Zaitsu, K. In *Ambient Ionization Mass Spectrometry in Life Sciences*, Zaitsu, K., Ed.; Elsevier: Amsterdam, 2020, pp 171-205.
(14) Sinclair, I.; Bachman, M.; Addison, D.; Rohman, M.; Murray, D. C.; Davies, G.; Mouchet, E.; Tonge, M. E.; Stearns, R. G.; Ghislain, L. Acoustic mist ionization platform for direct and contactless ultrahigh-throughput mass spectrometry analysis of liquid samples, *Anal. Chem.* **2019**, *91*, 3790-3794.
(15) Liu, P.; Zhang, J.; Ferguson, C. N.; Chen, H.; Loo, J. A. Measuring protein–ligand interactions using liquid sample desorption electrospray ionization mass spectrometry, *Anal. Chem.* **2013**, *85*, 11966-11972.
(16) Yao, C.; Wang, T.; Zhang, B.; He, D.; Na, N.; Ouyang, J. Screening of the binding of small molecules to proteins by desorption electrospray ionization mass spectrometry combined with protein microarray, *J. Am. Soc. Mass Spectrom.* **2015**, *26*, 1950-1958.
(17) Schultz, G. A.; Corso, T. N.; Prosser, S. J.; Zhang, S. A fully integrated monolithic microchip electrospray device for mass spectrometry, *Anal. Chem.* **2000**, *72*, 4058-4063.
(18) Van Pelt, C.; Zhang, S.; Henion, J. Characterization of a fully automated nanoelectrospray system with mass spectrometric detection for proteomic analyses, *J. Biomol. Tech.* **2002**, *13*, 72-84.
(19) Zhang, S.; Van Pelt, C. K.; Wilson, D. B. Quantitative determination of noncovalent binding interactions using automated nanoelectrospray mass spectrometry, *Anal. Chem.* **2003**, *75*, 3010-3018.
(20) Benkestock, K.; Van Pelt, C. K.; Åkerud, T.; Sterling, A.; Edlund, P.-O.; Roeraade, J. Automated nano-electrospray mass spectrometry for protein-ligand screening by noncovalent interaction applied to human H-FABP and A-FABP, *J. Biomol. Screen.* **2003**, *8*, 247-256.
(21) Jecklin, M. C.; Schauer, S.; Dumelin, C. E.; Zenobi, R. Label-free determination of protein-ligand binding constants using mass spectrometry and validation using surface plasmon resonance and isothermal titration calorimetry, *J. Mol. Recognit.* **2009**, *22*, 319-329.
(22) Maple, H. J.; Garlish, R. A.; Rigau-Roca, L.; Porter, J.; Whitcombe, I.; Prosser, C. E.; Kennedy, J.; Henry, A. J.; Taylor, R. J.; Crump, M. P. Automated protein–ligand interaction screening by mass spectrometry, *J. Med.Chem.* **2012**, *55*, 837-851.
(23) Woods, L. A.; Dolezal, O.; Ren, B.; Ryan, J. H.; Peat, T. S.; Poulsen, S.-A. Native state mass spectrometry, surface plasmon resonance, and X-ray crystallography correlate strongly as a fragment screening combination, *J. Med. Chem.* **2016**, *59*, 2192-2204.
(24) Göth, M.; Badock, V.; Weiske, J.; Pagel, K.; Kuropka, B. Critical evaluation of native electrospray ionization mass spectrometry for fragment‐based screening, *ChemMedChem* **2017**, *12*, 1201-1211.
(25) Schiebel, J.; Radeva, N.; Köster, H.; Metz, A.; Krotzky, T.; Kuhnert, M.; Diederich, W. E.; Heine, A.; Neumann, L.; Atmanene, C. One question, multiple answers: biochemical and biophysical screening methods retrieve deviating fragment hit lists, *ChemMedChem* **2015**, *10*, 1511-1521.
(26) Schiebel, J.; Radeva, N.; Krimmer, S. G.; Wang, X.; Stieler, M.; Ehrmann, F. R.; Fu, K.; Metz, A.; Huschmann, F. U.; Weiss, M. S. Six biophysical screening methods miss a large proportion of crystallographically discovered fragment hits: a case study, *ACS Chem. Biol.* **2016**, *11*, 1693-1701.
(27) Berndt, P.; Fattinger, C.; Steiner, R. System for dispensing a sample into a buffer liquid, US 9446408 B2, 2016.
(28) Neu, V.; Steiner, R.; Muller, S.; Fattinger, C.; Zenobi, R. Development and characterization of a capillary gap sampler as new microfluidic device for fast and direct analysis of low sample amounts by ESI-MS, *Anal. Chem.* **2013**, *85*, 4628-4635.
(29) Ghiasikhou, S.; da Silva, M. F.; Zhu, Y.; Zenobi, R. The capillary gap sampler, a new microfluidic platform for direct coupling of automated solid-phase microextraction with ESI-MS, *Anal. Bioanal. Chem.* **2017**, *409*, 6873-6883.
(30) Ghiasikhou, S.; Cazzamalli, S.; Scheuermann, J.; Neri, D.; Zenobi, R. Automated and enhanced extraction of a small molecule-drug conjugate using an enzyme-inhibitor interaction based SPME tool followed by direct analysis by ESI-MS, *Anal. Bioanal. Chem.* **2019**, *411*, 7387-7398.
(31) Neu, V.; Dörig, P.; Fattinger, C.; Müller, S.; Zenobi, R. Characterization of a miniaturized liquid bridge for nL sample infusion: a comparative study of sample flush-out behavior using flow simulations and direct ESI-MS analysis, *Microfluid. Nanofluidics* **2016**, *20*, 1-11.
(32) Ghiasikhou, S.; Marchand, A.; Zenobi, R. A comparative study between a miniaturized liquid junction built in a capillary gap and semi-open capillaries for nL sample infusion to mass spectrometry, *Microfluid. Nanofluidics* **2019**, *23*, 1-10.
(33) Gasteiger, E.; Hoogland, C.; Gattiker, A.; Wilkins, M. R.; Appel, R. D.; Bairoch, A. In *The proteomics protocols handbook*, Walker, J. M., Ed.; Humana Press: Totowa, 2005, pp 571-607.
(34) Kaeslin, J. The Gap Sampler: A Versatile Microfluidic Autosampler for Electrospray Ionization Mass Spectrometry, *Chimia* **2020**, *74*, 220-224.
(35) Chambers, M. C.; Maclean, B.; Burke, R.; Amodei, D.; Ruderman, D. L.; Neumann, S.; Gatto, L.; Fischer, B.; Pratt, B.; Egertson, J. A cross-platform toolkit for mass spectrometry and proteomics, *Nat. Biotechnol.* **2012**, *30*, 918-920.
(36) Liu, L.; Kitova, E. N.; Klassen, J. S. Quantifying protein-fatty acid interactions using electrospray ionization mass spectrometry, *J. Am. Soc. Mass Spectrom.* **2011**, *22*, 310-318.
(37) Daniel, J. M.; Friess, S. D.; Rajagopalan, S.; Wendt, S.; Zenobi, R. Quantitative determination of noncovalent binding interactions using soft ionization mass spectrometry, *Int. J. Mass Spectrom.* **2002**, *216*, 1-27.
(38) Tjernberg, A.; Markova, N.; Griffiths, W. J.; Hallén, D. DMSO-related effects in protein characterization, *J. Biomol. Screen.* **2006**, *11*, 131-137.
(39) Zhou, M.; Li, Q.; Kong, W.; Wang, R. In *Targeting Protein-Protein Interactions by Small Molecules*, Sheng, C.; Georg, G. I., Eds.; Springer: Singapore, 2018, pp 95-133.
(40) Kitova, E. N.; El-Hawiet, A.; Schnier, P. D.; Klassen, J. S. Reliable determinations of protein–ligand interactions by direct ESI-MS measurements. Are we there yet? , *J. Am. Soc. Mass Spectrom.* **2012**, *23*, 431-441.
(41) Landreh, M.; Alvelius, G.; Johansson, J.; Jörnvall, H. Protective effects of dimethyl sulfoxide on labile protein interactions during electrospray ionization, *Anal. Chem.* **2014**, *86*, 4135-4139.
(42) Supuran, C. T.; Casini, A.; Scozzafava, A. In *Carbonic anhydrase*, Supuran, C. T.; Scozzafava, A.; Conway, J., Eds.; CRC Press: Boca Raton, 2004, pp 67-147.
(43) Maren, T. H.; Conroy, C. W. A new class of carbonic anhydrase inhibitor, *J. Biol. Chem.* **1993**, *268*, 26233-26239.
(44) Zhang, J.-H.; Chung, T. D. Y.; Oldenburg, K. R. A Simple Statistical Parameter for Use in Evaluation and Validation of High Throughput Screening Assays, *J. Biomol. Screen.* **1999**, *4*, 67-73.